Sphere Packing Analysis for Performance Trade-off in Joint Communications and Sensing-Part I: General Principle

Husheng Li, Zhu Han, H. Vincent Poor

***Abstract*—Joint communications and sensing (JCS) provides an effective approach to enhance the spectral efficiency of wireless systems. When integrating these historically independent functions in the same waveform, both communication and sensing may suffer from performance degradation, thus resulting in a trade-off between their performances. A fundamental question is how to obtain bounds for the communication-sensing trade-off in JCS. In this paper, a geometric approach is adopted, namely evaluating the volume of a feasible waveform set given the tolerable performance degradation of sensing and then bounding the number of possible communication codewords using the sphere packing methodology. In particular, mathematical tools in high-dimensional geometry are leveraged for the volume calculation in the first of this paper. Applications for concrete sensing performance metrics will be left to the second part of the paper.**

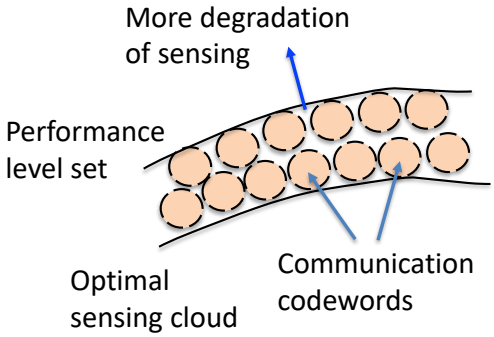

Fig. 1: Level sets and sphere packing.

I. Introduction

In recent years, joint communications and sensing (JCS) has received substantial attention due to the potential applications in 6G wireless networks and various cyber physical systems (CPSs). In JCS, both functions of communications and sensing are accomplished via the emission of the same waveform, thus saving significant power and spectrum. A convenient methodology is to reuse existing communication or sensing waveforms, such as orthogonal frequency division multiplexing (OFDM) and frequency modulation continuous wave (FMCW). For example, OFDM communication signal with modulating data (known to the JCS transceiver) can be considered as an OFDM radar waveform, while the parameters (e.g., the chirp rate) of FMCW radar can be modulated for conveying communication messages.

However, due to the conflict between the purposes of communications and sensing, there exists a trade-off between their performances, which has been studied by the first author [1]–[3] and other researchers [4]–[7]. Therefore, existing communication or sensing waveforms may not achieve the optimal performance since they are optimized for individual functions. Hence, in this paper, we study dedicated waveforms designed for JCS, which take the functional trade-off between communications and sensing into account. It is important to find bounds for performance metrics, such as the communication data rate, and ranging mean square error (MSE) or the ambiguity function (AF) for sensing, which can provide performance upper bounds and insights for the design of practical JCS waveforms.

To explicitly quantify the trade-off between communications and sensing in JCS, we use a geometric viewpoint. When we fix a value for the performance of sensing, the corresponding waveforms achieving the performance form a manifold in Euclidean space. Even the optimal waveform is not necessarily unique. For example, when the performance metric is the integrated sidelobe level (ISL) [8] in the autocorrelation function, which is expected to be small in order to reduce possible confusion between sidelobes and weak targets, the signal, as a vector, can be multiplied by a phase shift, without the loss of ISL performance. Therefore, the manifold of optimal sensing waveform is $[0, 2\pi]$, which allows phase shift keying (PSK) for communications. For the general case, the waveforms of the same performance metric form a level set, while the waveforms satisfying a performance guarantee, as the union of level sets, form a manifold of nonzero volume. Then, the data rate of communications is dependent on the volume of the sensing waveform

H. Li is with the School of Aeronautics and Astronautics, and the School of Electrical and Computer Engineering (email: husheng@purdue.edu). Z. Han is with the Department of Electrical Engineering, University of Houston (email: zhan2@uh.edu). H. V. Poor is with the Department of Electrical Engineering, Princeton University (email: poor@princeton.edu). This work was supported by the National Science Foundation under grants 2052780, 2135286, 2109295 and 2128455.

ICC 2024 - IEEE International Conference on Communications | 978-1-7281-9054-9/24/$31.00 ©2024 IEEE | DOI: 10.1109/ICC51166.2024.10622166

manifold. The greater the manifold volume is, the worse the sensing performance guarantee is, while more codewords with prescribed separation distance can be squeezed into the sensing waveform manifold, thus yielding a higher data rate. Using the sphere packing argument [9], bounds can be obtained for the communication data rate, given a sensing performance bound, and thus characterizing the performance trade-off between communications and sensing, as illustrated in Fig. 1. This geometric analysis directly relates data communication and radar sensing performance metrics, without the assumption of infinite codeword length in information theoretic argument, thus benefiting both fundamental research and practical interest.

The major challenge is how to evaluate the volume of the sensing waveform manifold. In the first part of this two-part paper, we will propose a generic framework for evaluating the volume of the feasible sensing waveform set, which will be applied to concrete sensing performance metrics in the second part of the paper.

The remainder of this paper is organized as follows. In Section II, existing researches related to this paper are briefly discussed. Then, the system model is introduced in Section III. The main part of this paper, namely the geometric analysis of the sensing waveform manifold and the generic principle of volume evaluation, is introduced in Section IV. Finally the numerical results and conclusions are given in Sections V and VI, respectively.

II. Related Works

Comprehensive surveys on the coexistence of communications and radar can be found in [10]–[14]. There have been substantial excellent studies on the fundamental performance evaluation of JCS. A rate-distortion theoretic argument is employed in [15] in a similar manner to the traditional rate-distortion theory for communications. In [16], [17], a multiple access channel is used to model the co-existence of communications and sensing, thus assessing the corresponding rate region. A related study on joint data transmission and channel state estimation can be found in [18]. The complexity analysis of the electromagnetic (EM) field is used to evaluate the degrees of freedom (DoF) of the field, which characterizes the trade-off between communications and sensing [3], [19]. Other studies on the trade-off between communications and sensing in JCS have been carried out; e.g., the conflict between the deterministic sensing waveform and random communication messages [6] and the compromise between the Cramér-Rao bound of sensing and the error exponent of communications [7]. Note that the concept of sphere packing has been employed in [4], [20] for JCS. However, the arguments therein are more qualitative, without an analytic calculation of the volumes.

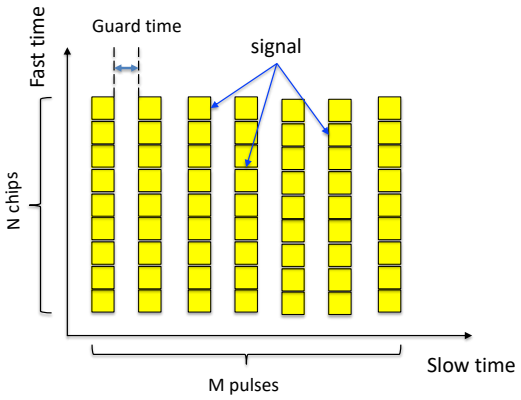

Fig. 2: Fast time and slow time data matrix.

III. System Model

In this section, we introduce the system model of JCS, without specifying the detailed schemes of modulation and coding.

A. Signal Model

For simplicity, we consider only ranging for the purpose of sensing. The proposed methodology in this paper can be extended to the estimation of angle of arrivals (AoA) and Doppler frequency shift, despite different details of calculations. The continuous-time signal within one pulse is denoted by $x(t)$. We assume N samples of $x(t)$ within one pulse, which are called chips and are denoted by $\mathbf{x} = (x_1, ..., x_N)^T$. The total available transmit power (normalized by the pulse duration) is denoted by P_t. We assume that $E[\|\mathbf{x}\|_2^2] = P_t$. Note that the instantaneous value $\|\mathbf{x}\|_2^2$ is not necessarily P_t. The chip period is denoted by T_c. Therefore, the signal bandwidth is approximately given by $W = \frac{1}{T_c}$. The waveform $\mathbf{x}$ is a function of the communication message. The frequency-spectrum signal, namely the Fourier transform of the time-domain signal $\mathbf{x}$, is denoted by $X(j\omega)$ or the discrete Fourier transform $\mathbf{X} = (X_1, ..., X_N)$, for continuous and discrete cases, respectively. As illustrated in Fig. 2, we consider M successive pulses along the slow time dimension. Therefore, the fast time (chips) and slow time (pulses) dimensions form a 2-dimensional matrix, over which the communication message is encoded, and the waveforms within different pulses could be different. The signal within the data matrix is denoted by $\bar{\mathbf{x}} = (\mathbf{x}_1, ..., \mathbf{x}_M)$, or equivalently $\bar{\mathbf{X}} = (\mathbf{X}_1, ..., \mathbf{X}_M)$.

We further assume that there are L distinct 2-dimensional waveforms for transmission. Each time the JCS transceiver selects one waveform to transmit, thus sending $R = \log_2 L$ bits. Therefore, each waveform can be considered as a codeword for communications, while the ensemble of waveforms corresponds to the codebook. For simplicity, we assume a single antenna at the transmitter and receiver. The extension

to MIMO cases needs nontrivial additional studies, which we plan to study in future work.

B. Performance Metrics

1) Communications: The performance of communications can be characterized by the data rate R and error probability p_e. When the Euclidean distance between two codewords (sensing waveforms) is d, while the noise is Gaussian with signal-to-noise ratio (SNR) γ, the error rate p_e of these two codewords is given by $p_e = Q\left(\frac{\sqrt{\gamma}d}{2}\right)$.

2) Sensing: In this paper, we consider the following two performance metrics of sensing:

- Ambiguity Function (AF): For single-antenna signals (thus being scalars), the performance of radar sensing is characterized by the AF proposed by Woodward [8], which is defined as

$$\chi(\tau,\nu) = \int_{-\infty}^{\infty} x(t)x^*(t-\tau)e^{-j2\pi\nu(t-\tau)}dt, \qquad (1)$$

  where x is the continuous-time transmitted scalar signal, τ is the time delay and ν is the Doppler-shift. The integral for continuous-time signal can be replaced by summation for discrete-time signal. The AF is expected to be peaky at the origin, and the sidelobes should be made as small as possible, in order to reduce the confusion of target. In this paper, we consider only the task of ranging. It simplifies the analysis in the discretize signals. The autocorrelation function of the discrete-time signal is given by

$$r[m] = \sum_{n=1}^{N-m} x_n x_{n+m}^*. \qquad (2)$$

  Note that $r[0] = P_t$. The normalized ISL [8] is defined as

$$\xi = \frac{\sum_{m=-(N-1)}^{N-1} |r[m]|^2 - |r[0]|^2}{|r[0]|^2}, \qquad (3)$$

  which is expected to be as low as possible.
- SNR: In the performance metric of ISL, the impact of noise is not taken into account. Therefore, an alternative and useful performance metric is the SNR, which is proportional to $\int P(j\omega)|H(j\omega)|^2 d\omega$. Then, the optimal PSD of the transmitted signal is given by

$$P_t^{opt}(j\omega) = \frac{|H(j\omega)|^2}{\int |H(j\phi)|^2 d\phi} P_t, \qquad (4)$$

  whose optimality is obviously guaranteed by the Cauchy-Schwartz inequality. Note that the PSD $P(j\omega)$ is in the average sense. For each communication symbol (radar pulse), the instantaneous PSD is not necessarily $P(j\omega)$. The discrete version of the optimal power allocation is

$$P_{t,n}^{opt} = \frac{|H_n|^2 P_t}{\sum_{m=1}^{N} |H_m|^2}. \qquad (5)$$

Note that other possible performance metrics include MSE [21] and signal-to-clutter ratio [22]. The proposed framework also applies to these performance metrics.

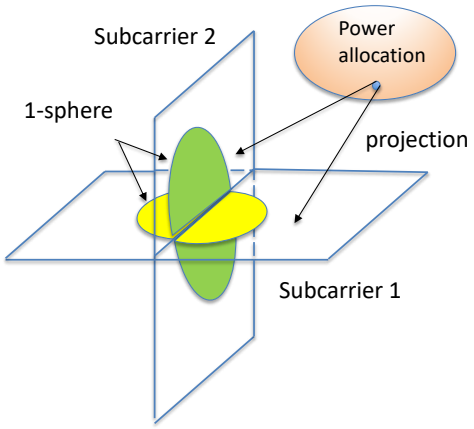

Fig. 3: Projections to subspaces.

IV. Structure of Feasible Waveform Set

In this section, we discuss the structure of the feasible waveform set, in which the codewords can be selected. The clarified geometric structure will be employed in the concrete analysis in Part 2 of this paper. We notice that the signal structure has a two-layer structure, in which the higher layer is the power allocation over different frequencies (or subcarriers in the terminology of OFDM) and the lower layer is the detailed signaling within each subcarrier, as illustrated in Fig. 3.

A. Fixed Power Allocation

Given a power allocation to each subcarrier $\{P_{t,n}\}_{n=1,...,N}$. The corresponding codeword on subcarrier n is denoted by $\bar{X} = \{X_{mn}\}_{m=1,...,M,n=1,...,N}$, where the coding is over the whole fast time and slow time data matrix. The projections of each codeword $\bar{\mathbf{X}}$ as a vector to subspace $\mathbf{X}_n = (X_{1,n}, ..., X_{M,n})$ (the n-th subcarrier), denoted by $\mathcal{P}_n(\mathbf{X})$, falls on the M-dimensional complex sphere $\mathcal{S}^M_{\sqrt{MP_{t,n}}}$, as illustrated in Fig. 3.

Then, the feasible waveform set is given by the product of the M-dimensional spheres corresponding to each subcarrier:

$$\begin{aligned}\mathbf{\Sigma}_x &= \left\{\mathbf{z}|\mathbf{z} \in \mathcal{S}^{MN}_{\sqrt{MP_t}}, \mathcal{P}_n(\mathbf{z}) = \mathcal{S}^M_{\sqrt{MP_{t,n}}}, n = 1, ..., N\right\} \\ &= \prod_{n=1}^{N} \mathcal{S}^M_{\sqrt{MP_{t,n}}}, \end{aligned} \qquad (6)$$

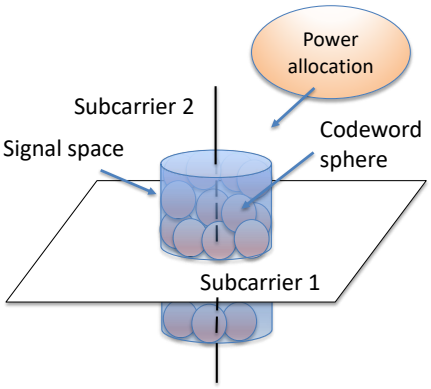

Fig. 4: An illustration of the product waveform set.

An illustration of the product waveform set is illustrated in Fig. 4, where the the dimensions of subcarriers 1 and 2 are 2 and 1, respectively, thus resulting in a 3-dimensional cylinder. The volume of complex sphere $\mathcal{S}^M_{\sqrt{MP_{t,n}}}$ is equal to that of real sphere $\mathbb{S}^{2M}_{\sqrt{MP_{t,n}}}$. Therefore, the volume of the feasible waveform set $\mathbf{\Sigma}_x$, whose real-valued dimension is $2MN$, is the product of each signal sphere of each subcarrier, given by the standard formula of sphere volume:

$$V(\mathbf{\Sigma}) = \frac{\pi^{MN}}{\Gamma^N(M+1)} M^{MN} \prod_{n=1}^{N} (P_{t,n})^M. \tag{7}$$

B. Flexible Power Allocation

For the case of multiple possible power allocations, the product structure of the feasible waveform set is no longer valid. An illustration for two possible power allocations is given in Fig. 5. The corresponding feasible waveform set is the union of two cylinders. When the possible power allocation is a non-discrete subset, the feasible waveform set, as the union of all feasible waveform sets corresponding to each power allocation, could be very complicated, which makes the explicit description prohibitive, needless to say the volume evaluation. Therefore, we have to consider a manipulable subset of the entire feasible waveform set.

To this end, we consider the sphere packing in the space of power allocation, as illustrated in Fig. 6. For the feasible set of power allocation denoted by $\mathbf{\Sigma}_P$, we consider a $\|\cdot\|_1$ sphere packing with radius $\frac{d^2}{2M}$. Then, we consider two power allocations $\mathbf{P}^1 = (P^1_{t,1}, ..., P^1_{t,N})$ and $\mathbf{P}^2 = (P^2_{t,1}, ..., P^2_{t,N})$ in different spheres, which satisfy

$$\sum_{n=1}^{N} |P^1_{t,n} - P^2_{t,n}| \geq \frac{d^2}{M\lambda}, \tag{8}$$

where the parameter λ is defined as

$$\lambda = \inf_{\mathbf{P}} \frac{\sum_{n=1}^{N} \left| \sqrt{P^1_{t,n}} - \sqrt{P^2_{t,n}} \right|^2}{\sum_{n=1}^{N} |P^1_{t,n} - P^2_{t,n}|}. \tag{9}$$

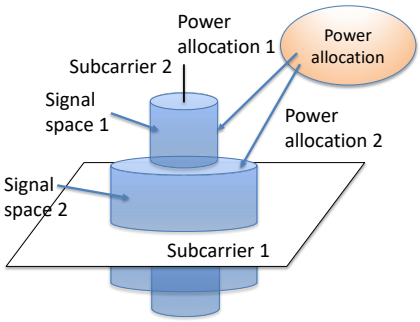

Fig. 5: Waveform sets corresponding to two different power allocations.

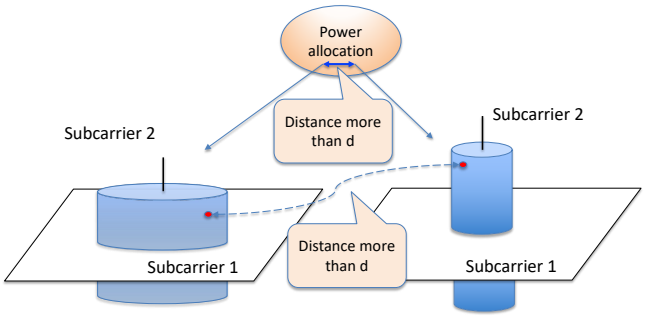

Fig. 6: Sphere packing in the power allocation space.

We assume that $\lambda > 0$, which is difficult to prove rigorous but can be justified by numerical results.

Then, for two waveforms $\bar{\mathbf{X}}_1$ and $\bar{\mathbf{X}}_2$, satisfying the power allocations $\mathbf{P}^1$ and $\mathbf{P}^2$, respectively, we have

$$\begin{aligned}
\|\bar{\mathbf{X}}_1 - \bar{\mathbf{X}}_2\|_2^2 &= \sum_{n=1}^{N}\sum_{m=1}^{M} |X^1_{mn} - X^2_{mn}|^2 \\
&\geq \sum_{n=1}^{N} \left| \sqrt{\sum_{m=1}^{M} |X^1_{mn}|^2} - \sqrt{\sum_{m=1}^{M} |X^2_{mn}|^2} \right|^2 \\
&= M \sum_{n=1}^{N} \left| \sqrt{P^1_{t,n}} - \sqrt{P^2_{t,n}} \right|^2 \\
&\geq M\lambda \sum_{n=1}^{N} |P^1_{t,n} - P^2_{t,n}| \geq d^2,
\end{aligned} \tag{10}$$

where the first inequality is due to the triangle inequality and the last inequality is due to (8). This implies

$$\|\bar{\mathbf{X}}_1 - \bar{\mathbf{X}}_2\|_2 \geq d. \tag{11}$$

Then, we can design one sub-codebook for each sphere in the power allocation space and use the union of the sub-codebook as the final codebook for JCS. If we guarantee that the codewords in each sub-codebook are separated by a Euclidean distance of at least d, then the d-separation also holds for the final codebook.

C. Sphere Packing: Gilbert–Varshamov Bound

We only derive lower bounds for the codebook size using a sphere packing argument, in a similar manner to the Gilbert–Varshamov bound [9]. To this end, we denote by $d_{\min}$ the minimum Euclidean distance between any pair of codewords. The number of codewords in the maximum codebook is denoted by $L(d_{\min})$. Then, any point in the waveform space should be contained within the sphere centered at a codeword and of radius $d_{\min}$. Otherwise, we can add this point to the codebook without violating the definition of $d_{\min}$, thus conflicting with the assumption of maximum codebook. Hence, the volume sum of the spheres centered at the codewords and with radius $d_{\min}$ is greater than the volume of the feasible waveform set.

1) Fixed Power Allocation: For the fixed power allocation, we obtain the following lower bound for the codebook size:

$$L(d_{\min}) \geq \frac{V(\mathbf{\Sigma}_x)}{V\left(\mathbb{S}_{d_{\min}}^{2MN}\right)}, \tag{12}$$

for which we need to evaluate the total volume $\mathbf{\Sigma}_x$ and the volume of the $2MN$-dimensional[1] real sphere $\mathbb{S}_{d_{\min}}^{2MN}$ with radius $d_{\min}$.

2) Flexible Power Allocation: For the flexible power allocation, we first carry out sphere packing for the power allocation space with radius $\frac{d_{\min}^2}{M\lambda}$[2]. The number of such spheres is lower bounded by $\frac{V(\mathbf{\Sigma}_P)}{V\left(\mathbb{S}_{\frac{d_{\min}^2}{M\lambda}}^{N}\right)}$. For each N-dimensional sphere in the power allocation space, we design a sub-codebook with minimum distance $d_{\min}$. The inequality (11) guarantees that the minimum distance of the final codebook, as the union of the sub-codebooks, is lower bounded by $d_{\min}$. Hence, the lower bound of the codebook size is given by

$$|\text{codebook}| \geq \frac{V(\mathbf{\Sigma}_P)}{V\left(\mathbb{S}_{\frac{d_{\min}^2}{M\lambda}}^{N}\right)} \frac{V(\mathbf{\Sigma}_x)}{V\left(\mathbb{S}_{d_{\min}}^{2MN}\right)}. \tag{13}$$

The sets $\mathbf{\Sigma}_x$, $\mathbb{S}_{\frac{d_{\min}^2}{M\lambda}}^{N}$ and $\mathbb{S}_{d_{\min}}^{2MN}$ are spheres, whose volumes can be easily calculated. The major challenge is the computation of the volume of the feasible power allocation space.

D. Volume of Generic Intersections

For a generic performance metric θ of sensing (the greater, the better), as a function of the power allocation $\mathbf{P}$, the feasible power allocation set $\mathcal{F}$ is defined by the level set of θ:

$$\mathcal{F} = \{\mathbf{P} | \theta(\mathbf{P}) \geq \theta_{opt} - \Delta\theta\}, \tag{14}$$

[1]The MN-dimensional complex sphere is $2MN$-dimensional in the real space.

[2]Here we assume that the performance degradation $\delta\gamma$ is sufficiently small and each optimal power allocation $P_{t,n}^{opt}$ is sufficiently large, such that all the power allocations in each sphere are nonnegative.

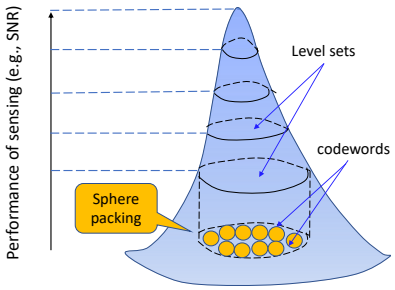

Fig. 7: Intersection of level set and power constraint.

where $\Delta\theta$ is the tolerable performance degradation of sensing. Meanwhile, the total transmit power should not change. Therefore, we have the linear constraint $\sum_{n=1}^{N} P_{t,n} = P_t$ as a hyperplane $\mathcal{P}$. Thus, the volume of the feasible power allocation set is the intersection of the level set $\mathcal{F}$ and the hyperplane $\mathcal{P}$:

$$\mathbf{\Sigma}_x = \mathcal{F} \cap \mathcal{P}. \tag{15}$$

For the volume evaluation of the interaction of a set and a hyperplane, we need the following theorem which provides a formula for calculating the the volume using Fourier transform. The volume calculation of intersections between hyperplanes and generic convex bodies can also be found in [23].

Theorem 1 (Theorem 3.2 in [23])**.** *For every $\xi = (\xi_1, ..., \xi_n) \in \mathbb{S}^{n-1}$, where $\mathbb{S}^{n-1}$ is the $n-1$-dimensional real sphere, and every $q > 0$, the volume of the intersection of the n-dimensional sphere B_q^n with norm $\|\cdot\|_q$ and the hyperplane $\xi^{\perp}$ perpendicular to ξ is given by*

$$\begin{aligned} & Vol_{n-1}(B_q^n \cap \xi^{\perp}) \\ = \; & \frac{q}{\pi(n-1)\Gamma\left(\frac{n-1}{q}\right)} \int_0^{\infty} \prod_{k=1}^{n} \gamma_q(t\xi_k) dt, \end{aligned} \tag{16}$$

where γ_q is the Fourier transform of the function $e^{-|\cdot|^q}$.

V. Numerical Results

We consider a JCS system in the 2.5GHz band with a bandwidth of 400MHz. We assume that the target is 100m away from the JCS transceiver. The target is assumed to be a ball with radius of 0.3m. Since the target size is comparable with the wavelength (0.12m at 2.5GHz), the reflection of the target is frequency-selective.

We evaluated the value of λ defined in (9), which is difficult to assess analytically. For different levels of deviation from the optimal power allocation, quantified by the power allocation variance, we randomly sample 100,000 sets of power allocation and evaluate the value of λ. The results are shown in Fig. 8, where we empirically observe that a larger deviation results in greater values of positive λ.

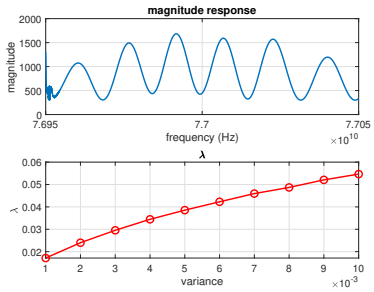

Fig. 8: Numerical evaluation of parameter λ.

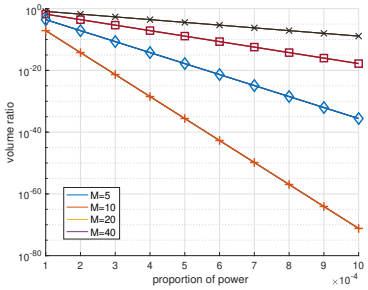

Fig. 9: Proportion of inner sphere for different values of M.

In the theoretical analysis, we relaxed the transmit power constraint, such that the transmitter does not necessarily transmit with peak power. The argument is that most of the volume (thus the codewords) is concentrated near the boundary. To verify this assumption, we plotted the volume ratio of waveform set with power $(1-\eta)P_t$ and P_t versus different values of η, when η is very small. Figure 9 shows that the number of codewords not close to the boundary is negligible, unless M is small.

VI. Conclusions

In this paper, we have studied the fundamental trade-off between communications and sensing in JCS systems. We have started from the set of optimal sensing waveforms, and discussed the volume of optimal waveforms for constructing the communication codebook. We have proposed a general principle for evaluating the volume of feasible waveform set for sensing, based on which the sphere-packing argument yields bounds for the data communication rate, thus characterizing the trade-off between communications and sensing in JCS. The concrete computation for specific sensing performance metrics will be left to the second part of this paper [24].

References

[1] H. Li, "Performance trade-off in inseparable joint communications and sensing: A pareto analysis," in *Proc. IEEE International Conference on Communications (ICC)*, 2022.

[2] ——, "Conflict and trade-off of waveform uncertainty in joint communication and sensing systems," in *Proc. IEEE International Conference on Communications (ICC)*, 2022.

[3] ——, "Degrees of freedom in scattered fields for trade-off in joint communications and sensing," in *Proc. IEEE International Conference on Communications*, 2022.

[4] Y. Xiong, F. Liu, Y. Cui, W. Yuan, T.-X. Han, and G. Caire, "On the fundamental tradeoff of integrated sensing and communications under Gaussian channels," *IEEE Trans. Info. Theory*, vol. under review, 2023.

[5] M. Chang, T. Erdogan, S. Wang, and M. R. Bloch, "Rate and detection error-exponent tradeoffs of joint communications and sensing," in *Proc. 2nd IEEE International Online Symposium on Joint Communications & Sensing (JC&S)*, 2021.

[6] F. Liu, Y. Xiong, K. Wan, T. X. Han, and G. Caire, "Deterministic-random tradeoff of integrated sensing and communications in gaussian channels: A rate-distortion perspective," 2023, pp. arxiv, https://arxiv.org/abs/2212.10 897.

[7] Z. Ren, X. Song, Y. Fang, L. Qiu, and J. Xu, "Fundamental CRB-rate trade-off in multi-antenna multicast channel with ISAC," in *Proc. IEEE Global Communication Conference*, 2022.

[8] J. L. H. He and P. Stoica, *Waveform Design for Active Sensing Systems: A Computational Approach*. Cambridge University Press, 2012.

[9] J. H. van Lint, *Introduction to Coding Theory*. Springer, 1992, vol. GTM 86.

[10] L. Han and K. Wu, "Joint wireless communication and radar sensing systems–state of the art and future prospects," *IET Microwaves, Antennas & Propagation*, vol. 7, no. 11, pp. 876–885, 2013.

[11] B. Paul, A. R. Chiriyath, and D. W. Bliss, "Survey of rf communications and sensing convergence research," *IEEE Access*, vol. 5, pp. 252–270, 2016.

[12] L. Zheng, M. Lops, Y. C. Eldar, and X. Wang, "Radar and communication co-existence: An overview," *arXiv preprint arXiv:1902.08676*, 2019.

[13] F. Liu, C. Masouros, A. Petropulu, H. Griffiths, and L. Hanzo, "Joint radar and communication design: Applications, state-of-the-art, and the road ahead," *IEEE Transactions on Communications*, 2020.

[14] D. Ma, N. Shlezinger, T. Huang, Y. Liu, and Y. C. Eldar, "Joint radar-communications strategies for autonomous vehicles," *IEEE Signal Processing Magazine*, vol. 37, no. 4, pp. 85–97, 2020.

[15] M. Kobayashi, H. Hamad, G. Kramer, and G. Caire, "Joint state sensing and communication over memoryless multiple access channels," *Proc. IEEE International Symposium on Information Theory (ISIT)*, pp. 270–274, 2019.

[16] A. R. Chiriyath, B. Paul, G. M. Jacyna, and D. W. Bliss, "Inner bounds on performance of radar and communications co-existence," *IEEE Transactions on Signal Processing*, vol. 64, no. 2, pp. 464–474, 2015.

[17] A. R. Chiriyath, B. Paul, and D. W. Bliss, "Radar-communications convergence: Coexistence, cooperation, and co-design," *IEEE Transactions on Cognitive Communications and Networking*, vol. 3, no. 1, pp. 1–12, 2017.

[18] W. Zhang, S. Vedantam, and U. Mitra, "Joint transmission and state estimation: A constrained channel coding approach," *IEEE Transactions on Information Theory*, vol. 57, no. 10, pp. 7084–7095, 2011.

[19] H. Li, "Dual function trade-off in joint communications and radar: An electromagnetic field analysis," in *Proc. IEEE Global Communication Conference*, 2021.

[20] X. Shen, N. Zhao, and Y. Shen, "On the performance tradeoff of an isac system with finite blocklength," in *arxiv*, 2023.

[21] M. I. Skolnik, *Introduction to Radar Systems (3rd edition)*. Mcgraw-Hill College, 2000.

[22] U. Pillai, K. Y. Li, I. Selesnick, and B. Himed, *Waveform Diversity: Theory and Applications*. McGraw Hill, 2011.

[23] A. Koldobsky, *Fourier Analysis in Convex Geometry*. American Mathematical Society, 2005.

[24] H. Li, Z. Han, and H. V. Poor, "Sphere packing analysis for performance trade-off in joint communications and sensing-part ii: Fourier analysis of volume," in *submitted to IEEE Global Communications Conference (Globalcom)*, 2023.